Research Article | Vol. 8, No. 8 | 1 Aug 2018 | OPTICAL MATERIALS EXPRESS 2035
Optical Materials EXPRESS

Selective IR response of highly textured phase change VO_2 nanostructures obtained via oxidation of electron beam deposited metallic V films

MERVE ERTAS USLU,[1,2] I. BURC MISIRLIOGLU,[1,2,3] AND KURSAT SENDUR[1,2,*]

[1]*Faculty of Engineering and Natural Sciences, Sabancı University, Orhanlı/Tuzla 34956 Istanbul, Turkey*
[2]*Sabancı University Nanotechnology Application Center, Orhanlı/Tuzla, 34956 Istanbul, Turkey*
[3]*Integrated Manufacturing Technologies Research and Application Center, Sabanci University, Tuzla, 34956 Istanbul, Turkey*
[*]*sendur@sabanciuniv.edu*

Abstract: We demonstrate the growth of highly textured VO_2 nanocrystals via annealing of e-beam deposited amorphous metallic V. Temperature dependent ellipsometry results reveal the pronounced reflection near the IR spectrum above the transition and an almost temperature independent weak reflection in the visible spectrum. The IR reflection displays a strong hysteresis during heating and cooling near the transition temperature at 68°C, indicating a first order transition and a strain-free structure. Our work demonstrates the feasibility to obtain high quality phase change nanostructures that transmit the visible spectrum but reflect IR and is suitable for large scale fabrication.

OCIS codes: (160.6840) Thermo-optical materials; (310.6845) Thin film devices and applications; (310.6860) Thin films, optical properties; (130.4815) Optical switching devices.

References and links

1. F. Morin, "Oxides which show a metal-to-insulator transition at the Neel temperature," Phys. Rev. Lett. **3**(1), 34–36 (1959).
2. M. Marezio, D. B. McWhan, J. Remeika, and P. Dernier, "Structural Aspects of the Metal-Insulator Transitions in Cr-Doped VO2," Phys. Rev. B **5**(7), 2541–2551 (1972).
3. Y. Dachuan, X. Niankan, Z. Jingyu, and Z. Xiulin, "Vanadium dioxide films with good electrical switching property," J. Phys. D Appl. Phys. **29**(4), 1051–1057 (1996).
4. A. Tselev, I. A. Luk'yanchuk, I. N. Ivanov, J. D. Budai, J. Z. Tischler, E. Strelcov, A. Kolmakov, and S. V. Kalinin, "Symmetry relationship and strain-induced transitions between insulating M1 and M2 and metallic R phases of vanadium dioxide," Nano Lett. **10**(11), 4409–4416 (2010).
5. A. Tselev, E. Strelcov, I. A. Luk'yanchuk, J. D. Budai, J. Z. Tischler, I. N. Ivanov, K. Jones, R. Proksch, S. V. Kalinin, and A. Kolmakov, "Interplay between ferroelastic and metal-insulator phase transitions in strained quasi-two-dimensional VO2 nanoplatelets," Nano Lett. **10**(6), 2003–2011 (2010).
6. J. Zhou, Y. Gao, Z. Zhang, H. Luo, C. Cao, Z. Chen, L. Dai, and X. Liu, "VO_2 thermochromic smart window for energy savings and generation," Sci. Rep. **3**(1), 3029 (2013).
7. X. Chen, Q. Lv, and X. Yi, "Smart window coating based on nanostructured VO_2 thin film," Optik (Stuttg.) **123**(13), 1187–1189 (2012).
8. S. Babulanam, T. Eriksson, G. Niklasson, and C. Granqvist, "Thermochromic VO_2 films for energy-efficient windows," Sol. Energy Mater. **16**(5), 347–363 (1987).
9. C. G. Granqvist and G. A. Niklasson, "Thermochromic oxide-based thin films and nanoparticle composites for energy-efficient glazings," Buildings **7**(1), 3 (2016).
10. M. Saeli, C. Piccirillo, M. Warwick, and R. Binions, "Thermochromic thin films: synthesis, properties and energy consumption modelling," in *Materials and Processes for Energy: Communicating Current Research and Technological Developments,* A. Mendez-Vilas, ed. (Formatex Research Center, 2013), pp.736–746.
11. H. Kim, N. Charipar, E. Breckenfeld, A. Rosenberg, and A. Piqué, "Active terahertz metamaterials based on the phase transition of VO_2 thin films," Thin Solid Films **596**, 45–50 (2015).
12. S. K. Earl, T. D. James, T. J. Davis, J. C. McCallum, R. E. Marvel, R. F. Haglund, Jr., and A. Roberts, "Tunable optical antennas enabled by the phase transition in vanadium dioxide," Opt. Express **21**(22), 27503–27508 (2013).

#325405 https://doi.org/10.1364/OME.8.002035
Journal © 2018 Received 15 Mar 2018; revised 21 Jun 2018; accepted 22 Jun 2018; published 2 Jul 2018

Optical Materials EXPRESS

13. Y.-G. Jeong, H. Bernien, J.-S. Kyoung, H.-R. Park, H.-S. Kim, J.-W. Choi, B.-J. Kim, H.-T. Kim, K. J. Ahn, and D.-S. Kim, "Electrical control of terahertz nano antennas on VO_2 thin film," Opt. Express **19**(22), 21211–21215 (2011).
14. M. J. Dicken, K. Aydin, I. M. Pryce, L. A. Sweatlock, E. M. Boyd, S. Walavalkar, J. Ma, and H. A. Atwater, "Frequency tunable near-infrared metamaterials based on VO2 phase transition," Opt. Express **17**(20), 18330–18339 (2009).
15. J. Lappalainen, S. Heinilehto, S. Saukko, V. Lantto, and H. Jantunen, "Microstructure dependent switching properties of VO_2 thin films," Sens. Actuators A Phys. **142**(1), 250–255 (2008).
16. T.-H. Yang, S. Nori, H. Zhou, and J. Narayan, "Defect-mediated room temperature ferromagnetism in vanadium dioxide thin films," Appl. Phys. Lett. **95**(10), 102506 (2009).
17. H. Zhou, M. F. Chisholm, T.-H. Yang, S. J. Pennycook, and J. Narayan, "Role of interfacial transition layers in VO2/Al2O3 heterostructures," J. Appl. Phys. **110**(7), 073515 (2011).
18. J. Montero, Y.-X. Ji, S.-Y. Li, G. A. Niklasson, and C. G. Granqvist, "Sputter deposition of thermochromic VO_2 films on In_2O_3: Sn, SnO_2, and glass: Structure and composition versus oxygen partial pressure," J. Vac. Sci. Technol. B Nanotechnol. Microelectron. **33**(3), 031805 (2015).
19. P. Jin, K. Yoshimura, and S. Tanemura, "Dependence of microstructure and thermochromism on substrate temperature for sputter-deposited VO_2 epitaxial films," J. Vac. Sci. Technol. A **15**(3), 1113–1117 (1997).
20. Y. Luo, S. Pan, S. Xu, L. Zhong, H. Wang, and G. Li, "Influence of sputtering power on the phase transition performance of VO_2 thin films grown by magnetron sputtering," J. Alloys Compd. **664**, 626–631 (2016).
21. M. Taha, S. Walia, T. Ahmed, D. Headland, W. Withayachumnankul, S. Sriram, and M. Bhaskaran, "Insulator-metal transition in substrate-independent VO_2 thin film for phase-change devices," Sci. Rep. **7**(1), 17899 (2017).
22. M. Yang, Y. Yang, B. Hong, L. Wang, K. Hu, Y. Dong, H. Xu, H. Huang, J. Zhao, H. Chen, L. Song, H. Ju, J. Zhu, J. Bao, X. Li, Y. Gu, T. Yang, X. Gao, Z. Luo, and C. Gao, "Suppression of Structural Phase Transition in VO_2 by Epitaxial Strain in Vicinity of Metal-insulator Transition," Sci. Rep. **6**(1), 23119 (2016).
23. L. Fan, S. Chen, Y. Wu, F. Chen, W. Chu, X. Chen, C. Zou, and Z. Wu, "Growth and phase transition characteristics of pure M-phase VO_2 epitaxial film prepared by oxide molecular beam epitaxy," Appl. Phys. Lett. **103**(13), 131914 (2013).
24. J. Leroy, A. Bessaudou, F. Cosset, and A. Crunteanu, "Structural, electrical and optical properties of thermochromic VO2 thin films obtained by reactive electron beam evaporation," Thin Solid Films **520**(14), 4823–4825 (2012).
25. V. Théry, A. Boulle, A. Crunteanu, J.-C. Orlianges, A. Beaumont, R. Mayet, A. Mennai, F. Cosset, A. Bessaudou, and M. Fabert, "Structural and electrical properties of large area epitaxial VO_2 films grown by electron beam evaporation," J. Appl. Phys. **121**(5), 055303 (2017).
26. R. Marvel, K. Appavoo, B. Choi, J. Nag, and R. Haglund, "Electron-beam deposition of vanadium dioxide thin films," Appl. Phys., A Mater. Sci. Process. **111**(3), 975–981 (2013).
27. Z. Zhang, Y. Gao, Z. Chen, J. Du, C. Cao, L. Kang, and H. Luo, "Thermochromic VO_2thin films: solution-based processing, improved optical properties, and lowered phase transformation temperature," Langmuir **26**(13), 10738–10744 (2010).
28. L. Kang, Y. Gao, and H. Luo, "A novel solution process for the synthesis of VO_2 thin films with excellent thermochromic properties," ACS Appl. Mater. Interfaces **1**(10), 2211–2218 (2009).
29. Z. Chen, Y. Gao, L. Kang, J. Du, Z. Zhang, H. Luo, H. Miao, and G. Tan, "VO_2-based double-layered films for smart windows: optical design, all-solution preparation and improved properties," Sol. Energy Mater. Sol. Cells **95**(9), 2677–2684 (2011).
30. X. Cao, N. Wang, J. Y. Law, S. C. J. Loo, S. Magdassi, and Y. Long, "Nanoporous thermochromic VO_2 (M) thin films: controlled porosity, largely enhanced luminous transmittance and solar modulating ability," Langmuir **30**(6), 1710–1715 (2014).
31. L. Kang, Y. Gao, Z. Zhang, J. Du, C. Cao, Z. Chen, and H. Luo, "Effects of annealing parameters on optical properties of thermochromic VO_2 films prepared in aqueous solution," J. Phys. Chem. C **114**(4), 1901–1911 (2010).
32. S. Lu, L. Hou, and F. Gan, "Structure and optical property changes of sol-gel derived VO_2 thin films," Adv. Mater. **9**(3), 244–246 (1997).
33. T. Maruyama and Y. Ikuta, "Vanadium dioxide thin films prepared by chemical vapour deposition from vanadium (III) acetylacetonate," J. Mater. Sci. **28**(18), 5073–5078 (1993).
34. M. Sahana, G. Subbanna, and S. Shivashankar, "Phase transformation and semiconductor-metal transition in thin films of VO_2 deposited by low-pressure metalorganic chemical vapor deposition," J. Appl. Phys. **92**(11), 6495–6504 (2002).
35. H. K. Kim, H. You, R. P. Chiarello, H. L. Chang, T. J. Zhang, and D. J. Lam, "Finite-size effect on the first-order metal-insulator transition in VO_2 films grown by metal-organic chemical-vapor deposition," Phys. Rev. B Condens. Matter **47**(19), 12900–12907 (1993).
36. D. Malarde, M. J. Powell, R. Quesada-Cabrera, R. L. Wilson, C. J. Carmalt, G. Sankar, I. P. Parkin, and R. G. Palgrave, "Optimized Atmospheric-Pressure Chemical Vapor Deposition Thermochromic VO_2 Thin Films for Intelligent Window Applications," ACS Omega **2**(3), 1040–1046 (2017).
37. M. E. A. Warwick, I. Ridley, and R. Binions, "Thermochromic vanadium dioxide thin films prepared by electric field assisted atmospheric pressure chemical vapour deposition for intelligent glazing application and their energy demand reduction properties," Sol. Energy Mater. Sol. Cells **157**(Supplement C), 686–694 (2016).

Optical Materials EXPRESS

38. D. Graf, J. Schläfer, S. Garbe, A. Klein, and S. Mathur, "Interdependence of Structure, Morphology, and Phase Transitions in CVD Grown VO_2 and V_2O_3 Nanostructures," Chem. Mater. **29**(14), 5877–5885 (2017).
39. M. Yang, Y. Yang, B. Hong, L. Wang, K. Hu, Y. Dong, H. Xu, H. Huang, J. Zhao, H. Chen, L. Song, H. Ju, J. Zhu, J. Bao, X. Li, Y. Gu, T. Yang, X. Gao, Z. Luo, and C. Gao, "Suppression of Structural Phase Transition in VO_2 by Epitaxial Strain in Vicinity of Metal-insulator Transition," Sci. Rep. **6**(1), 23119 (2016).
40. E. Breckenfeld, H. Kim, K. Burgess, N. Charipar, S.-F. Cheng, R. Stroud, and A. Piqué, "Strain Effects in Epitaxial VO_2 Thin Films on Columnar Buffer-Layer TiO_2/Al_2O_3 Virtual Substrates," ACS Appl. Mater. Interfaces **9**(2), 1577–1584 (2017).
41. M. Nakano, D. Okuyama, K. Shibuya, M. Mizumaki, H. Ohsumi, M. Yoshida, M. Takata, M. Kawasaki, Y. Tokura, T. Arima, and Y. Iwasa, "Distinct Substrate Effect on the Reversibility of the Metal–Insulator Transitions in Electrolyte-Gated VO_2Thin Films," Adv Electron Mater **1** (7), 1500093-n/a (2015).
42. D. Lee, J. Lee, K. Song, F. Xue, S.-Y. Choi, Y. Ma, J. Podkaminer, D. Liu, S.-C. Liu, B. Chung, W. Fan, S. J. Cho, W. Zhou, J. Lee, L.-Q. Chen, S. H. Oh, Z. Ma, and C.-B. Eom, "Sharpened VO_2 Phase Transition via Controlled Release of Epitaxial Strain," Nano Lett. **17**(9), 5614–5619 (2017).
43. C. Wan, E. Horak, J. King, J. Salman, Z. Zhang, Y. Zhou, P. Roney, B. Gundlach, S. Ramanathan, and R. Goldsmith, "Limiting optical diodes enabled by the phase transition of vanadium dioxide," *arXiv preprint* arXiv:1801.06728 (2018).
44. Y. Cui and S. Ramanathan, "Substrate effects on metal-insulator transition characteristics of rf-sputtered epitaxial VO2 thin films," J. Vac. Sci. Technol. A **29**(4), 041502 (2011).
45. H.-T. Zhang, L. Zhang, D. Mukherjee, Y.-X. Zheng, R. C. Haislmaier, N. Alem, and R. Engel-Herbert, "Wafer-scale growth of VO2 thin films using a combinatorial approach," Nat. Commun. **6**(1), 8475 (2015).
46. N. Bahlawane and D. Lenoble, "Vanadium oxide compounds: structure, properties, and growth from the gas phase," Chem. Vap. Depos. **20** (7–8-9), 299–311 (2014).
47. C. O. F. Ba, S. T. Bah, M. D'Auteuil, V. Fortin, P. V. Ashrit, and R. Vallée, "VO_2 thin films based active and passive thermochromic devices for energy management applications," Curr. Appl. Phys. **14**(11), 1531–1537 (2014).
48. J. Y. Suh, R. Lopez, L. C. Feldman, and R. Haglund, Jr., "Semiconductor to metal phase transition in the nucleation and growth of VO_2 nanoparticles and thin films," J. Appl. Phys. **96**(2), 1209–1213 (2004).
49. T.-H. Yang, R. Aggarwal, A. Gupta, H. Zhou, R. J. Narayan, and J. Narayan, "Semiconductor-metal transition characteristics of VO_2 thin films grown on c-and r-sapphire substrates," J. Appl. Phys. **107**(5), 053514 (2010).
50. J. K. Kana, J. Ndjaka, G. Vignaud, A. Gibaud, and M. Maaza, "Thermally tunable optical constants of vanadium dioxide thin films measured by spectroscopic ellipsometry," Opt. Commun. **284**(3), 807–812 (2011).
51. A. Zimmers, L. Aigouy, M. Mortier, A. Sharoni, S. Wang, K. G. West, J. G. Ramirez, and I. K. Schuller, "Role of thermal heating on the voltage induced insulator-metal transition in VO_2," Phys. Rev. Lett. **110**(5), 056601 (2013).
52. D. J. Hilton, R. P. Prasankumar, S. Fourmaux, A. Cavalleri, D. Brassard, M. A. El Khakani, J. C. Kieffer, A. J. Taylor, and R. D. Averitt, "Enhanced photosusceptibility near Tc for the light-induced insulator-to-metal phase transition in vanadium dioxide," Phys. Rev. Lett. **99**(22), 226401 (2007).
53. A. Facchetti and T. Marks, "*Transparent electronics: from synthesis to applications"*, John Wiley & Sons (2010).
54. T. D. Manning, I. P. Parkin, R. J. Clark, D. Sheel, M. E. Pemble, and D. Vernadou, "Intelligent window coatings: atmospheric pressure chemical vapour deposition of vanadium oxides," J. Mater. Chem. **12**(10), 2936–2939 (2002).
55. A. Makarevich, I. Sadykov, D. Sharovarov, V. Amelichev, A. Adamenkov, D. Tsymbarenko, A. Plokhih, M. Esaulkov, P. Solyankin, and A. Kaul, "Chemical synthesis of high quality epitaxial vanadium dioxide films with sharp electrical and optical switch properties," J. Mater. Chem. C Mater. Opt. Electron. Devices **3**(35), 9197–9205 (2015).
56. R. Minch and M. Es-Souni, "Nanostructured VO_2 thin films via cathodic deposition," CrystEngComm **15**(34), 6645–6647 (2013).
57. H. W. Liu, L. M. Wong, S. J. Wang, S. H. Tang, and X. H. Zhang, "Ultrafast insulator–metal phase transition in vanadium dioxide studied using optical pump–terahertz probe spectroscopy," J. Phys. Condens. Matter **24**(41), 415604 (2012).
58. N. Pertsev, A. Zembilgotov, and A. Tagantsev, "Effect of mechanical boundary conditions on phase diagrams of epitaxial ferroelectric thin films," Phys. Rev. Lett. **80**(9), 1988–1991 (1998).
59. A. P. Levanyuk, and A. S. Sigov, *Defects and Structural Phase Transitions* (Routledge, 1988).
60. M. J. Miller, "Advancements in Optical Properties of Thermochromic VO2 Films through Experimental and Numerical Investigations," Dissertation, University of Washington (2016).

1. Introduction

Tailoring electronic structure transitions to tune optical properties is a route provided by only a few transition metal oxides classified as phase change materials. Vanadium dioxide (VO_2) is among these materials and has attracted widespread interest recently due its well-known insulator-to-metal transition (IMT). IMT in VO_2 was first reported in 1959 by Morin [1] and

Optical Materials EXPRESS

this system possesses a phase transition of electronic origin. VO_2 is thermodynamically stable with monoclinic crystal structure with an energy gap of 0.7 eV below the critical temperature (T_C) of 68°C [2]. Above this temperature, VO_2 converts to rutile crystal structure accompanied by a metallic-like state leading to abrupt changes in electrical and optical properties. The emergence of free carriers in the conduction band brings the VO_2 from a transparent state (when below T_C) to a reflecting state (above T_C). The electrical resistance of VO_2 in the metallic phase is reduced by 4-5 orders of magnitude [3]. VO_2 has also attracted attention not only for its electronic transition, which is a result of structural change, but also for its phase co-existence under elastic clamping as demonstrated by Tselev et al. [4, 5].

With the ever increasing need for materials with new functionalities for integrated circuits and smart surface technologies, VO_2 has entered the agenda of groups focusing on applications and device design. Some interesting examples include thermochromic smart window coatings [6–10], tunable antennas [11–13], tunable metamaterials [14], and electronic switch components [15] in integrated circuits. VO_2 can be synthesized both in bulk powder form as well as in thin film form. As the latter is more suitable option for a variety of applications pertaining to device design and surfaces, many groups have investigated the growth of VO_2 films using pulsed laser deposition (PLD) [16, 17], magnetron sputtering [18–22], molecular beam epitaxy (MBE) [23], e-beam deposition [24–26], sol-gel [27–32] and CVD [33–38] methods. Some of these attempts also focused on the effect of strain via the choice of the substrate on the phase transition characteristics of this system [39–44], while there was at least one work attempting to utilize the MBE method that is known for small scale film growth to obtain high quality VO_2 films on large area substrate [45]. Obtaining high-quality VO_2 films indispensable for high-tech applications is a problem because V can form stable oxides such as V_2O_3, V_2O_5 and V_6O_{13} [46], i.e., stoichiometries other than VO_2. Controlling the optical response via tailoring the electronic transition of VO_2 appears as a feasible option, prompting a number of research groups to explore this opportunity in the past few years. A recently emerging potential area of application exploiting the IMT of VO_2 is the thermal management of devices and structures [47]. Such efforts have been the driving force behind a number of scientific studies to understand the characteristics of VO_2 especially when in thin film form.

Suh, Lopez et al. fabricated the VO_2 samples on Si substrate by PLD technique, followed by thermal oxidation to create VO_2 crystal form. They showed that when the semiconductor to metal transition, the width of the reflectivity hysteresis loop at the transition temperature was visible with increasing grain size in VO_2 films and nanoparticles [48]. Apart from implying a first order transition that occurs in nanofilms when clamping effects are negligible, this can be understood as hysteresis of any thermodynamic first order derivative or second order derivative property could originate from the overheating and undercooling as a result of barrier to nucleation. The barrier to nucleating of the new phase can be overcome only via overheating (when going from low symmetry to high symmetry phase) or undercooling (when going from high symmetry to low symmetry phase) where metastable states can exist around the thermodynamic transition point. Aggarwal et al. have grown epitaxial VO_2 films on c- and r-sapphire substrates and investigated the relationship between the growth orientations and the influence of texture on phase transition behavior. They showed that the thermal hysteresis and the transition for VO_2 films on c-sapphire was much more prominent and sharp than those of VO_2 films on r-sapphire, a possible implication of the effect of elastic misfit strains on the transition characteristics. The reason for this difference in IMT characteristics has been explained on the basis of lower grain boundary energy and higher in-plane misorientation in VO_2 films grown on c-sapphire [49]. Kana, Ndjaka et al. deposited VO_2 thin film on glass substrates by radio frequency inverted cylindrical magnetron sputtering. They demonstrated the active modulations of optical constants of VO_2 thin film through controlling the external temperature. They have studied both theoretically and experimentally the relation between the hysteresis loop, which shows the structural phase transition, and the optical constant of VO_2

Optical Materials EXPRESS

comparatively [50]. Zimmers et al. deposited VO_2 thin films on r-cut sapphire substrate with a magnetron sputter method and then performed four-probe measurements by forming patterns on the surface to describe the dc voltage induced switching mechanism. They reported that the main mechanism for the dc voltage or dc current induced insulator-metal transition in VO_2 is due to local heating and not a purely electronic effect [51] where they claim that the temperature rise needed for the transition can be provided simply by the intrinsic resistance leading to Joule heating. Hilton group measured the time-dependent conductivity of VO_2 during a photoinduced IMT where they observed a decrease in the necessary flux of photons to induce the metallic phase [52]. These works indicate that the source of the heat necessary to raise the temperature of the VO_2 structure to induce the IMT can have various origins, pointing out to the wide range of applications for this material.

In this paper we report on VO_2 nanostructures grown on [001] Si substrate through annealing of amorphous metallic V films initially grown with e-beam deposition. The controlled Ar atmosphere annealing of the metallic amorphous V generated strain-free structures almost homogeneous in grain size that display the characteristics of stress-free VO_2. Formation of the monoclinic VO_2 by annealing can facilitate a novel route to create surfaces with optical functionality. We found that e-beam evaporation growth of metallic V and followed by an annealing treatment is practical and straightforward and could be a cheaper option compared or obtaining VO_2 unlike other vacuum coating methods like magnetron sputtering, PLD etc., where precise monitoring of several growth parameters during the process is essential. The technique we used in this work is a thermal evaporation technique where the power is supplied by an energetic electron beam [53]. Thermal evaporation techniques are suitable for large area deposition on substrates. Following the growth of these structures, we carried out structural (XRD and Raman spectroscopy) and temperature dependent ellipsometry experiments that reveal a distinct electronic transition in our samples. While we observe the similarities in reflectivity data of our samples with those reported in the literature around the IMT, our samples display a pronounced lower reflectivity in the visible regime. We discussed the implications of the transition characteristics and the spectrum dependent behavior of the reflectivity in the context of optical scattering processes.

2. Experimental methods

VO_2 nanostructure films were fabricated by first depositing metallic V films on [001] Si substrate using Torr e-beam evaporation at room temperature. Fabrication of the V thin film was carried out at room temperature by using high purity V (99.9%) as a target placed in the crucible. For metallic V deposition, we chose a W e-beam crucible to deposit because of the high melting point (1890°C) of V. The target was bombarded by an e-beam in a chamber with a base pressure better than 3 $x10^{-6}$ Torr and the growth pressure in this work was kept at 6.9 $x10^{-6}$ Torr. Film growth rate was tracked by a quartz based thickness monitor to be around 0.5 Å/s. Metallic V growth was followed by heat treatment at 700°C under controlled Ar gas (purity 99.8%) at a flow rate of 2L/min through a 40 mm diameter quartz tube Prior to metallic V depositing, Si substrate was ultrasonically cleaned in acetone followed by isopropyl alcohol for 30 min to remove all contamination and finally dried in a nitrogen atmosphere.

Optical Materials EXPRESS

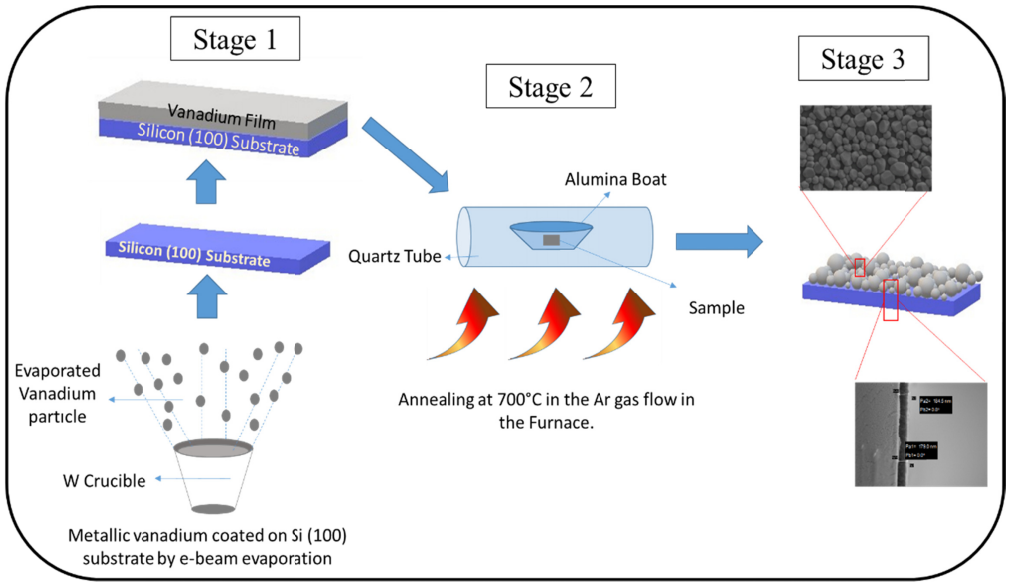

Fig. 1. The schematic illustration of the fabrication process. The schematic illustration of the fabrication process is shown in Fig. 1. Here, Stage 1 in Fig. 1, we illustrated depositing of V thin film on Si substrate using W e-beam crucible. Then, we illustrated annealing step at 700°C under Ar gas flow of V thin film sample by placing alumina boat in quartz tube in Stage 2. Finally, VO_2 nano-crystalline formed after annealing is illustrated base on the SEM image in Stage 3.

The crystal structure and growth orientation of the prepared sample was characterized by X-ray diffraction (XRD) under Cu Kα radiation (1.5418 Å) in a 2θ range varying from 10° to 90° using a Bruker diffractometer. Raman scattering spectroscopy was used to confirm the VO_2 phase at room temperature using Renishaw inVia Reflex Raman Spectrometer with a 532 nm laser beam in the range of 110-990 cm^{-1}. The laser was focused on the sample with a 50x objective. Surface morphology, and grain size distributions of the prepared samples were analyzed by a scanning electron microscopy (SEM) instrument at an accelerating voltage of 5kV (model FEG-SEM Leo Supra 35 and Bruker Flash). Spectral reflectivity measurements were performed with a WASE 400 ellipsometery as a function of temperature for unpolarized light incident at 30° in the wavelength range of 300 to 2100 nm allowing us to probe the near UV and far IR frequency response of our samples.

3. Results and discussion

To determine the crystal structure of the films before (as grown) and after heat treatment, θ-2θ X-ray diffraction (XRD) measurements were acquired for the VO_2 film after annealing as shown in Fig. 2. Since the growth of the metallic V was carried out at room temperature, the V cannot form the crystal phase due to lack of thermally activated diffusion. This state of V being far from equilibrium acts as the driving force for crystallization accompanied by the formation of VO_2 during the heat treatment at 700°C. In Fig. 2, we note that the peak located at 2θ = 27.89° corresponds to the monoclinic VO_2 (011) orientation. The inset in Fig. 2 is shown to illustrate the rather sharp nature of this peak pointing out to the presence of highly crystalline VO_2. Absence of peaks other than VO_2 (011) implies that our films highly textured. The best lattice match between VO_2 and Si occurs in a [011] VO_2// [002] Si orientation relationship, which is also what we encounter in our films. In the XRD measurements, we did not observe any diffraction peaks associated with metallic V or oxide compositions with stoichiometries other than VO_2. This indicates that the homogeneous VO_2 can be obtained via oxidation of metallic V films on large area substrates without the need for

Optical Materials EXPRESS

expensive and complex film deposition techniques. As seen in the inset of Fig. 2, the well-defined characteristic sharp XRD peak at 2θ = 27.89° obtained from the annealed sample indicate that VO_2 structures are highly crystalline.

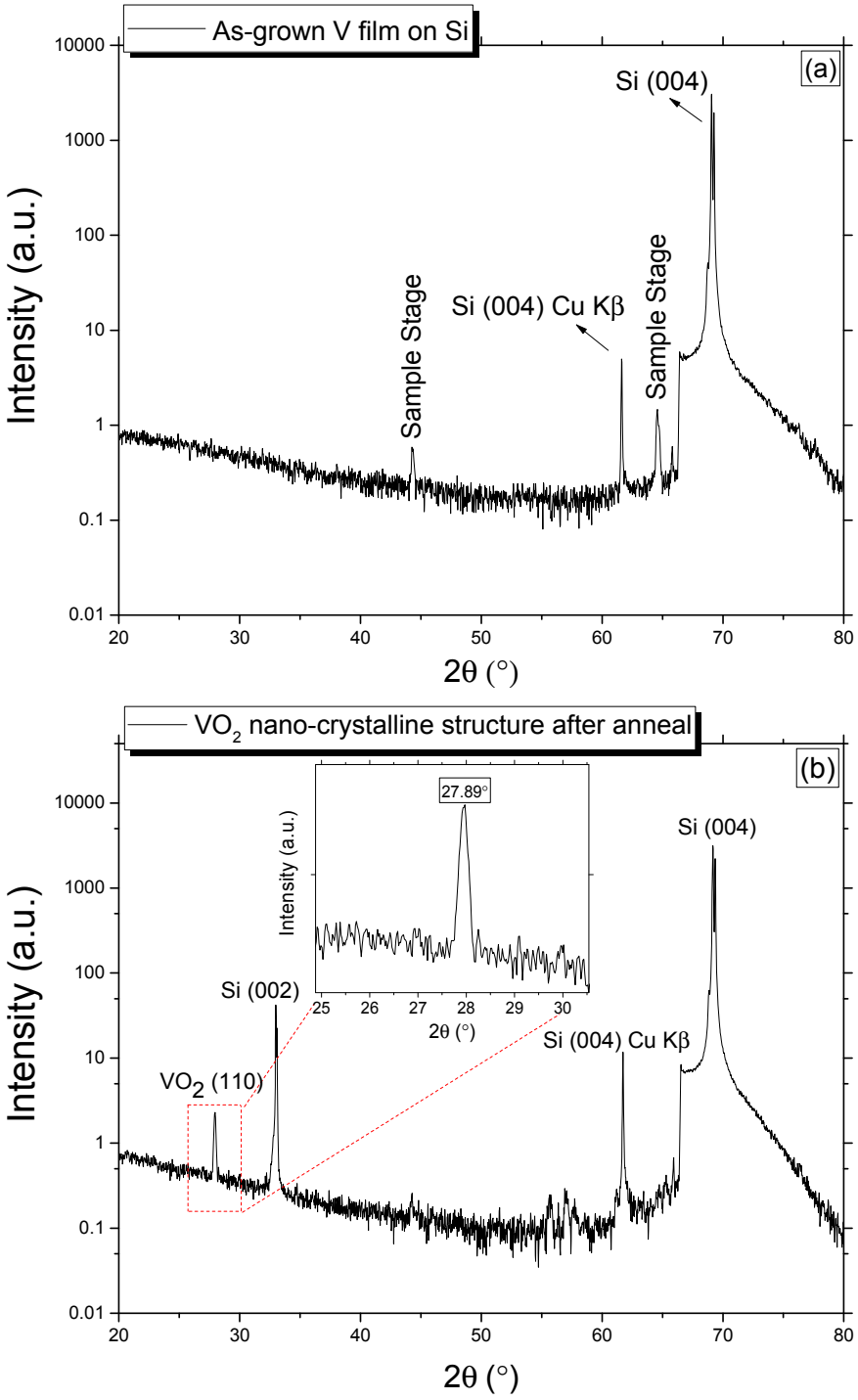

Fig. 2. θ-2θ X-ray diffraction (XRD) patterns of (a) the as-grown V film on Si (001) and (b) after heat treatment of the as-grown V film.

Optical Materials EXPRESS

In parallel with XRD measurements, we also carried out Raman spectroscopy characterization of the post-deposition annealed VO_2 nanostructures fabricated on Si to confirm the presence of the VO_2 phase. These results are shown in Fig. 3. In the spectral results, we were able to clearly assign the peak position at 142, 192, 223, 260, 309, 339, 389, 497, 613 cm^{-1} to V-O and V-V [54–57] characteristic vibration modes respectively that are both associated with the monoclinic phase, except the Si peak at 520 cm^{-1} which originated from the substrate.

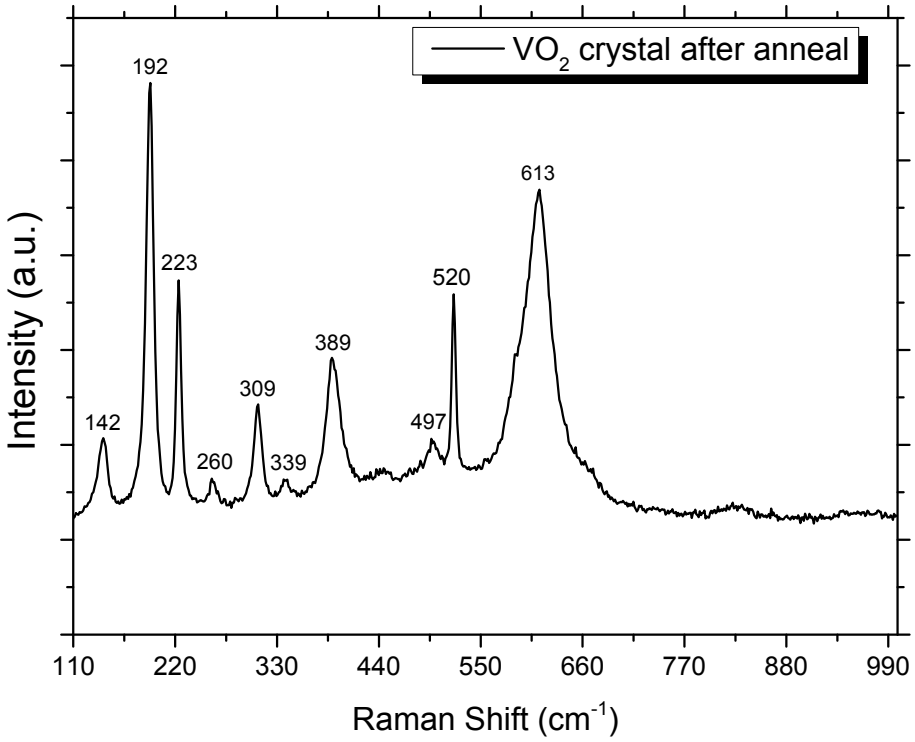

Fig. 3. Raman spectroscopy results of the post-deposition annealed VO_2 nanostructure fabricated on Si.

Following structural assessment of our samples, we carried out scanning electron microscope (SEM) analysis to visualize the morphological aspects. Figure 4 shows the SEM images revealing the surface morphology of the as-grown V film sample and the same sample following annealing at 700°C for 120 min. It can be seen that the surface morphology of as-grown V film sample shows an almost featureless surface with very small variations in morphology. After annealing these structures at 700°C for 120 min, a densely dispersed crystalline nanostructure is formed (Figs. 4(c)-(d)) on the surface with a small variation in particle size. The as-grown V film and VO_2 layer thicknesses are presented using cross section SEM image in Fig. (b) and (e). It was observed that heat treatment at 700°C resulted in a dramatic decrease in film thickness from 548 nm (as-grown V thin film) to 182 nm (VO_2 layer), displaying the extent of a possible volume change in a structure when it goes from an amorphous to crystalline form accompanied by a stoichiometry change.

Optical Materials EXPRESS

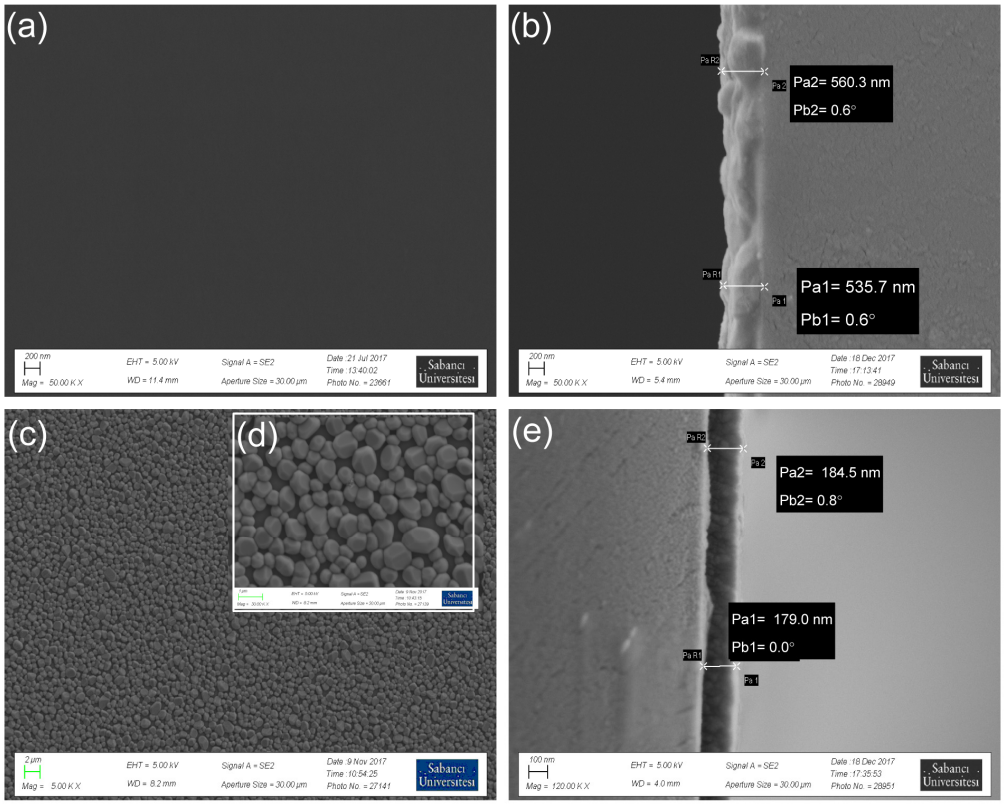

Fig. 4. SEM images for V deposited thin film (a) surface image, (b) cross section SEM image to analysis thickness, after that sample annealed to form VO_2 layer (c) and (d) surface image, (e) cross section SEM image.

As we observed that our samples consist of homogeneously distributed nano islands of VO_2 over the Si surface, we expected to observe some changes in the critical temperature as well as a smearing of the transition. This expectation was not fulfilled as we shall discuss. In Fig. 5, we provide the spectral reflectivity results, which are obtained using temperature dependent ellipsometer measurements during heating/cooling for VO_2 layer. The reflectivity curves are obtained from the VASE system that we utilize, which measures the reflectivity directly at different wavelengths and there is no further parametric fitting taking place in the experiments. The temperature is controlled using an in-house designed and built heater stage for the ellipsometer. In Fig. 5(a) and 5(c), we demonstrate the spectral reflectivity of the structures in heating and cooling cycles, respectively. The insets given in Figs. 5(b) and 5(d) shows the details in the visible part of the spectrum. It can be seen that at high temperatures our VO_2 layer provides a pronounced reflection of the incident radiation at infrared spectrum while the visible spectral reflection is both weak and is almost temperature independent. In the cooling cycle, spectral distribution at 80°C has a slight deviation from the spectral distribution of the high temperature curves. This happens in the first measurement of the cooling cycle, where the temperature control is relatively hard. The rest of the spectral curves are in accordance with the expectation for the high temperature regime. This result indicates that such structures will filter out IR wavelength when the VO_2 layer is heated to high temperatures, while transmitting the visible spectrum at all times. Such an outcome is promising especially for thermal management applications using smart materials and coatings. Note that the behavior in the visible reflection is different than what has been reported in literature for solid VO_2 films. In literature, an increase in reflectivity in the visible

Optical Materials EXPRESS

regime accompanies the increase in temperature in contrast to what we observe in the results in Fig. 5. Note that the high temperature (> 68°C) reflectivity values in Fig. 5(a) and 5(c) are almost identical. The curves in 5 (c) corresponding to 62°C and 64°C are obtained during cooling and is a consequence of the 1st order transition behavior where the metallic state can persist for some amount of undercooling. We discuss the possible mechanism for the loss of visible spectrum reflection in the coming paragraphs.

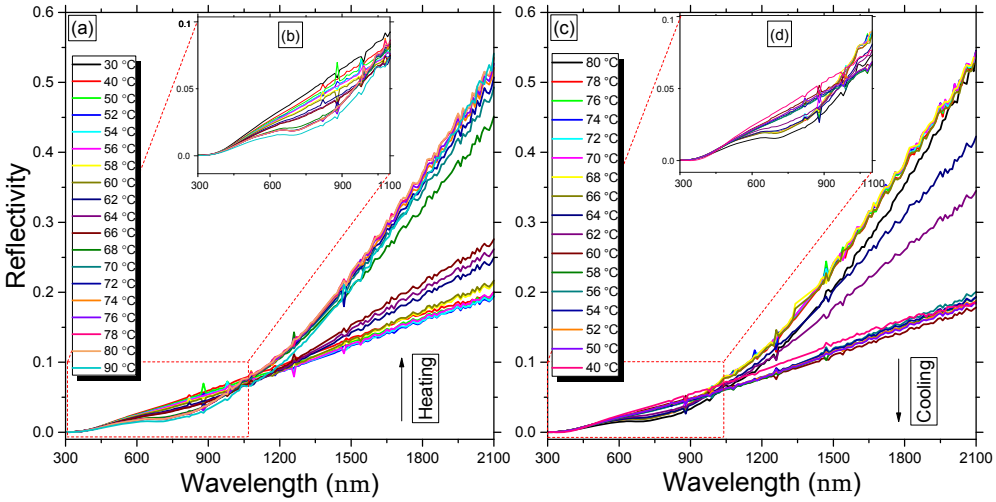

Fig. 5. Reflectivity spectrum for (a) the entire spectrum during heating, (b) visible spectrum (inset) during heating (c) the entire spectrum during cooling and (d) visible spectrum (inset) during cooling.

In Fig. 6, we provide the heating and cooling cycles in fixed wavelengths at infrared (2100 nm) and visible (700 nm). According to Fig. 6, as the temperature increases, the reflectivity rather abruptly increases after 68°C, particularly in the infrared region. This temperature corresponds to the IMT in VO_2 where the film passes from the monoclinic crystal structure to rutile upon heating accompanied by a change in carrier density. As one can clearly observe the transition with almost no smearing, it can be concluded that all VO_2 particles behave similarly. Such an outcome indicates that the nanoparticles are almost strain-free and do not suffer from any size-driven effects such as a reduction in transition temperature despite their nano-scale dimension. This phenomenon, i. e., size driven reduction of the transition temperature, is often reported in magnetic and ferroelectric systems where spin and electric ordering accompanies structural symmetry change in the lattice. As we shall show in the next paragraph, we see some hysteresis in the reflectivity around 68°C which indicates that the films are not only strain-free but are also clamping-free, undergoing a 1^{st} order phase transition as clamping of films undergoing structural transition is reported to reduce the transition to 2^{nd} order. Such behavior is analogous to ferroelectric thin films undergoing phase transition inducing symmetry changes in the unit cell are shown to exhibit this behavior where the jump in first order derivatives of the free energy disappear and are shifted to second order derivatives [58, 59].

Optical Materials EXPRESS

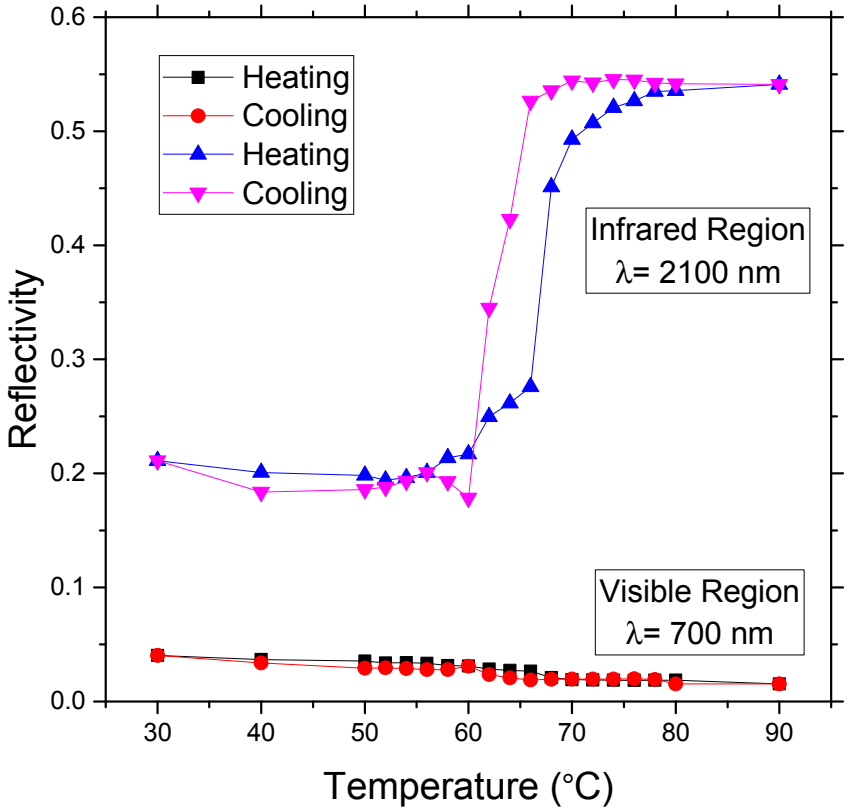

Fig. 6. The reflectivity data plotted as a function of temperature for the VO_2 structure on Si for the 2100 nm and 700 nm wavelengths. Notice the hysteresis in the former, a sign of a 1st order transition in the nanostructures indicating that the structures are clamping- and strain-free.

We also present the frequency dependent optical constants in Figs. 7(a) and 7(b) for two different temperatures corresponding to insulating and metallic phases in the IR region, respectively. We extracted the optical constant n and k from the spectral reflectivity data as given in Table 1. To achieve this, spectroscopic ellipsometry was used to measure the amplitude attenuation (ψ) and phase change (Δ) in the spectral range at incidence angles ranging from 30° to 45°, 5° increments. A basic spline (B-Spline) method was used to determine the n and k optical constant from the measured amplitude and polarization. The B-Spline method is a very flexible approach for modelling the refractive index and it is especially useful for absorbing materials such as the VO_2 [60]. In Table 1 we provide the optical constants at and beyond the near IR region, as the visible spectrum data cannot be explained by the fitting function. This approach assumes the presence of a homogeneously reflecting surface, which is fulfilled at longer wavelengths. Here, our goal is to shed light on the morphological dependence of the scattering process particularly in the visible regime. The resolution of the features decrease with increasing wavelength, a corollary of the Rayleigh criterion, which indicates that features much smaller than the wavelength will appear as a single homogeneous entity in the far field zone. As can be seen in Figs. 7(a) and 7(b), the variations in the optical constants are damped out, approaching the values of solid monolayer films. This indicates that the nanostructures displayed in Fig. 4(c) and 4(d) "appear" as a solid film to the IR regime of the incoming light, while the same structure behaves as an array of scatters to the wavelengths in the visible regime.

Optical Materials EXPRESS

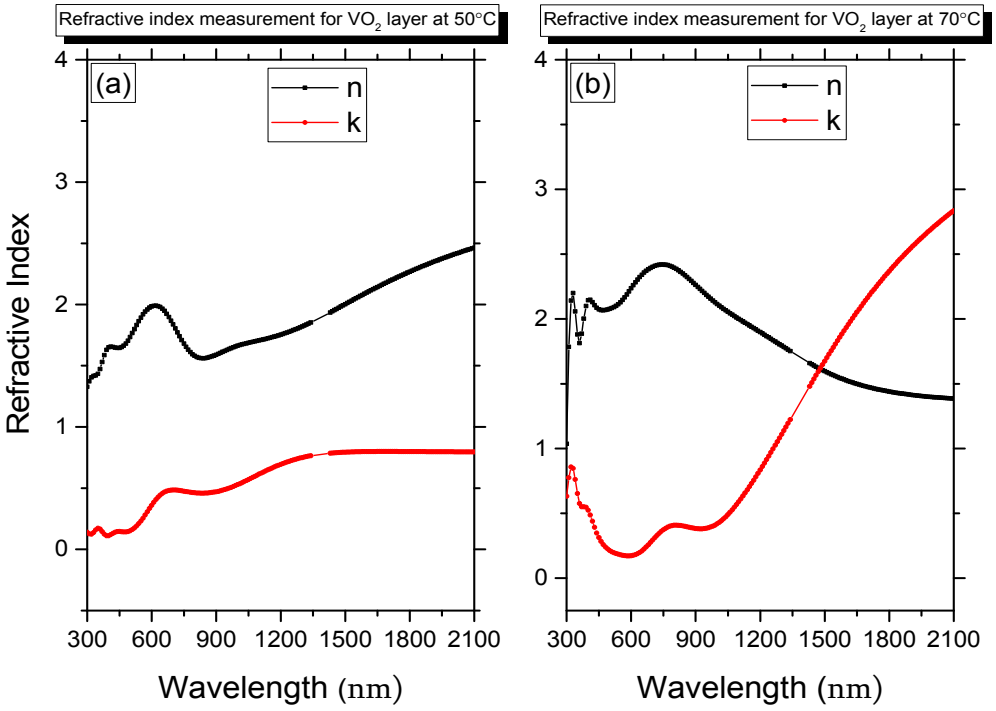

Fig. 7. Frequency dependent optical constants value for 2 different temperatures corresponding to (a) insulating (at 50°C) and (b) metallic (at 70°C) phases.

In the large wavelength regime (in the infrared), the incoming wave sees an almost homogeneous medium due to the small grain size (compared to wavelength). However, in the 300 to 400 nm wavelength regime, the wavelength is comparable to the grain size. The geometric dependent scattering and absorption effects become more prominent at this wavelength regime, therefore, increasing the effective optical loss constant of the medium accompanied by low reflectivity. However, the change in the effective optical loss constant upon IMT transition is rather small in the 300-400 nm regime compared to the infrared regime. We attribute the low reflectivity in the visible regime despite an apparent increase in k to geometric scattering effects when the wavelength of the incident radiation is comparable to the nano island size. Therefore, the overall reflectivity change upon IMT in the visible regime is much smaller than infrared. For long wavelengths, after the IMT transition as seen in Fig. 7(b), the value of n is comparable to or smaller than k, which leads to an enhanced reflectivity in the metallic state in the infrared frequencies that we observe in Fig. 5. For wavelengths comparable to grain size, the change in k for the metallic state compared to that of the insulator state is relatively small while n is almost constant. Therefore, the small wavelength reflectivity in both the metallic and the insulator states are more influenced by n. As a consequence, similar behavior in reflectivity for both states are observed in the visible.

Conclusion

In this study, we demonstrated that VO_2 nanocrystals with phase change response for optical applications can be obtained by annealing amorphous metallic V thin films. Our XRD results demonstrated a single VO_2 monoclinic (110) peak without any other undesired contributions from oxide phases of V. Using temperature dependent ellipsometer measurements, we demonstrated thermochromic and spectral properties of VO_2 crystalline nanostructures at various temperatures. Our experimental results showed a sudden increase in the infrared

Optical Materials EXPRESS

reflection above the IMT, while not affecting the reflection within the visible spectrum in almost the entire temperature range of interest in this work. Transition from the insulator phase to the metallic one is sharp, occurs around the bulk transition temperature and is accompanied by a prominent hysteresis, indicating that the nanostructures of VO_2 on Si are clamping- as well as strain-free. The overall reduction in the reflection of the visible regime from the surface can be explained on the basis of the surface morphology of our samples. The surface morphology dependence of the reflected spectrum intensity disappears in the IR regime as evidenced from the agreement of the optical constants extracted from our samples matching that of the homogeneous film results. Our experimental techniques could pave the way for easy, cheap, and mass production of phase change materials, which demonstrated desirable temperature dependent spectral features for energy applications.

Appendix

Table 1. Optical Constants of VO_2 Nanostructure of Materials (λ>1000 nm)

	Refractive index measurement for VO_2 layer at 50°C		Refractive index measurement for VO_2 layer at 70°C	
λ (eV)	n	k	n	K
1.23984	1.66315	0.52791	2.11485	0.41878
1.22757	1.66869	0.53585	2.10197	0.4302
1.21553	1.67376	0.54408	2.08958	0.44314
1.20373	1.67846	0.55255	2.07761	0.45748
1.19216	1.68286	0.56121	2.06599	0.47312
1.1808	1.68705	0.56999	2.05467	0.48995
1.16966	1.69108	0.57886	2.04359	0.50787
1.15873	1.69502	0.58777	2.03273	0.5268
1.148	1.69891	0.59667	2.02202	0.54665
1.13747	1.7028	0.60555	2.01146	0.56734
1.12713	1.70673	0.61435	2.00099	0.58881
1.11697	1.71073	0.62306	1.99061	0.61098
1.107	1.71483	0.63166	1.98029	0.63381
1.09721	1.71905	0.6401	1.97001	0.65723
1.08758	1.72342	0.64839	1.95976	0.68119
1.07812	1.72795	0.65649	1.94952	0.70565
1.06883	1.73265	0.66439	1.93928	0.73056
1.05969	1.73754	0.67209	1.92904	0.75589
1.05071	1.74263	0.67956	1.91878	0.78159
1.04188	1.74792	0.68679	1.90851	0.80764
1.0332	1.75343	0.69379	1.89821	0.834
1.02466	1.75914	0.70053	1.88789	0.86064
1.01626	1.76507	0.70703	1.87754	0.88755
1.008	1.77122	0.71326	1.86717	0.91469
0.99987	1.77758	0.71923	1.85677	0.94204
0.99187	1.78416	0.72494	1.84634	0.96958
0.984	1.79096	0.73038	1.83589	0.99729
0.97625	1.79797	0.73556	1.82542	1.02516
0.96863	1.80519	0.74048	1.81493	1.05316
0.96112	1.81261	0.74514	1.80443	1.08128
0.95372	1.82024	0.74953	1.79391	1.10951
0.94644	1.82807	0.75367	1.78339	1.13783

Optical Materials EXPRESS

0.93927	1.83609	0.75756	1.77287	1.16623
0.93221	1.8443	0.7612	1.76234	1.19469
0.92526	1.8527	0.7646	1.75183	1.2232
0.86702	1.93493	0.78551	1.65962	1.47992
0.861	1.94452	0.78698	1.65003	1.50812
0.85506	1.95415	0.78832	1.64064	1.5362
0.84921	1.96381	0.78955	1.63145	1.56413
0.84343	1.97349	0.79066	1.62248	1.5919
0.83773	1.98318	0.79167	1.61372	1.6195
0.83211	1.99287	0.79258	1.60519	1.6469
0.82656	2.00255	0.79341	1.59688	1.67411
0.82109	2.01222	0.79416	1.5888	1.7011
0.81569	2.02186	0.79483	1.58094	1.72787
0.81035	2.03148	0.79543	1.57331	1.75441
0.80509	2.04106	0.79596	1.56591	1.78071
0.7999	2.05061	0.79643	1.55873	1.80676
0.79477	2.0601	0.79685	1.55178	1.83255
0.78971	2.06955	0.79722	1.54504	1.85808
0.78471	2.07895	0.79754	1.53851	1.88334
0.77977	2.0883	0.79782	1.5322	1.90833
0.7749	2.09758	0.79806	1.52609	1.93304
0.77009	2.1068	0.79827	1.52018	1.95747
0.76533	2.11596	0.79844	1.51447	1.98162
0.76064	2.12505	0.79858	1.50895	2.00549
0.756	2.13407	0.79869	1.50361	2.02907
0.75142	2.14301	0.79877	1.49846	2.05237
0.74689	2.15189	0.79884	1.49348	2.07538
0.74242	2.16069	0.79888	1.48867	2.0981
0.738	2.16941	0.7989	1.48403	2.12053
0.73363	2.17805	0.79891	1.47955	2.14268
0.72932	2.18662	0.7989	1.47522	2.16454
0.72505	2.1951	0.79887	1.47104	2.18612
0.72084	2.20351	0.79883	1.46701	2.20742
0.71667	2.21183	0.79879	1.46312	2.22844
0.71255	2.22007	0.79873	1.45937	2.24918
0.70848	2.22823	0.79866	1.45574	2.26964
0.70446	2.23631	0.79859	1.45225	2.28983
0.70048	2.24431	0.79851	1.44887	2.30974
0.69654	2.25222	0.79842	1.44562	2.32939
0.69265	2.26005	0.79833	1.44248	2.34877
0.6888	2.2678	0.79823	1.43945	2.36789
0.685	2.27546	0.79813	1.43653	2.38675
0.68123	2.28304	0.79803	1.43371	2.40535
0.67751	2.29054	0.79792	1.43099	2.4237
0.67383	2.29796	0.79782	1.42837	2.4418
0.67018	2.3053	0.79771	1.42584	2.45965
0.66658	2.31255	0.7976	1.4234	2.47725
0.66302	2.31973	0.79749	1.42105	2.49462
0.65949	2.32682	0.79738	1.41878	2.51174

Optical Materials EXPRESS

0.656	2.33383	0.79728	1.41659	2.52864
0.65255	2.34076	0.79717	1.41448	2.5453
0.64913	2.34762	0.79707	1.41245	2.56173
0.64575	2.35439	0.79696	1.41048	2.57794
0.64241	2.36109	0.79686	1.40859	2.59393
0.63909	2.36771	0.79676	1.40677	2.6097
0.63582	2.37426	0.79667	1.40501	2.62525
0.63257	2.38073	0.79658	1.40332	2.64059
0.62936	2.38712	0.79649	1.40169	2.65573
0.62618	2.39344	0.7964	1.40011	2.67066
0.62304	2.39968	0.79631	1.3986	2.68539
0.61992	2.40586	0.79623	1.39714	2.69991
0.61684	2.41196	0.79615	1.39573	2.71425
0.61378	2.41798	0.79608	1.39438	2.72839
0.61076	2.42394	0.79601	1.39307	2.74234
0.60777	2.42983	0.79594	1.39182	2.7561
0.6048	2.43564	0.79588	1.39061	2.76968
0.60187	2.44139	0.79582	1.38945	2.78308
0.59896	2.44707	0.79577	1.38833	2.7963
0.59608	2.45268	0.79572	1.38725	2.80934
0.59323	2.45823	0.79567	1.38622	2.82221
0.5904	2.46371	0.79563	1.38522	2.83492

Funding

TUBITAK (115M033).